УДК 66.047

SIMULATION OF SPRAY EVAPORATION USING PRESSURE AND ULTRASONIC ATOMIZER – A COMPARATIVE ANALYSIS

Huang Lixin[1], K. Kumar[2], Arun S. Mujumdar[1]

Department of Mechanical Engineering, National University of Singapore (1), CFD Division, Institute of High Performance Computing (2)

Key words and phrases: CFD; droplet size distribution; nozzle; spray drying.

Abstract: Conventional pressure atomization imparts a high initial velocity to the droplets and also produces a wide droplet size distribution. If the jet is broken up with the assistance of ultrasonic energy finer droplets with a much more uniform size distribution can be obtained. Using the correlation of Rajan and Pandit [2001] which accounts for the physical-chemical properties of the liquid as well as the ultrasonic properties of the atomizer (amplitude, frequency, area of vibrating surface), a computational fluid dynamics (**CFD**) simulation was carried out to predict the spray evaporation performance in a co-current cylinder-on-cone spray chamber. The results are compared with those for a conventional pressure atomizer. The model predictions were validated by favorable comparison with literature data on velocity and temperature fields in a cylinder-on-cone chamber geometry. Since the ultrasonic nozzle has a low initial droplet velocity and a uniform size distribution, different droplet velocities (0.014, 5.59 and 59.0 m/s) and mean droplet sizes (10.0, 30.0, 50.0, 70.0, 90.0 and 110.0 μm) are used to simulate spray drying. The advantages and limitations of using ultrasonic atomizer rather than the conventional ones are discussed in the light of the simulation results.

Nomenclature

A_p – surface area of the droplet, m^2;

B_1, B_2, B_3 – Empirical parameters for $k-\varepsilon$ turbulence model;

C_D – drag coefficient;

C_s – moisture concentration at the droplet surface, $\mathrm{mol/m}^3$;

C_g – moisture concentration in the bulk gas, $\mathrm{mol/m}^3$;

D_m – diffusion coefficient of vapor in the bulk, m^2/s;

c_p – heat capacity of the droplet, $\mathrm{J/(kg \cdot K)}$;

d_p – droplet diameter, μm;

$\overline{d}$ – rosin-Rammler mean droplet diameter, μm;

$\frac{dm_p}{dt}$ – rate of evaporation, kg/s;

E – enthalpy of gas phase, $\mathrm{J/kg}$;

f – excitation frequency, HZ;

$\vec{g}$ – gravity vector, m^2/s;

G_k – production of turbulence kinetic energy due to the mean velocity gradients;

G_ε – production of turbulence kinetic energy due to buoyancy;

h – convective heat transfer coefficient, $\mathrm{W/(m^2 \cdot K)}$;

h_{fg} – latent heat, $\mathrm{J/kg}$;

H – Enthalpy of moisture, $\mathrm{J/kg}$;

J – diffusive mass flux of moisture, $\mathrm{kg/s}$;

k – turbulent kinetic energy, $\mathrm{m}^2/\mathrm{s}^2$;

k_c – mass transfer coefficient, $\mathrm{m/s}$;

k_{eff} – effective thermal conductivity of gas; $\mathrm{W/(m \cdot K)}$;

k_g – thermal conductivity of the hot medium, $\mathrm{W/(m \cdot K)}$;
m_p – mass of the droplet, kg;
$\overline{m_p}$ – average mass of the droplets in the control volume, kg;
Δm_p – change in the mass of the droplet in the control volume, kg;
$m_{p,0}$ – initial mass of the droplet, kg;
$\dot{m}_{p,0}$ – initial mass flow rate of the droplet injection tracked, $\mathrm{kg/s}$;
M_m – source term in continuity equation;
$\overrightarrow{M_F}$ – source term in momentum equation;
M_h – source term in energy equation;
N_i – molar flux of vapor, $\mathrm{mol/(m^2 \cdot s)}$;
$p_{\mathrm{sat}}(T_p)$ – saturated vapor pressure at the particle droplet temperature, Pa;
p_{op} – operating pressure, Pa;
P – pressure, Pa;
Q – volumetric flow rate of liquid, $\mathrm{kg/s}$;
R – universal gas constant, $\mathrm{J/(mol \cdot K)}$;
S_k – user-defined source term;
S_ε – user-defined source term;
t – time s;
T – temperature, K;
T_g – gas temperature, K;
$\overrightarrow{u_g}$ – gas velocity vector, $\mathrm{m/s}$;
$\overrightarrow{u_p}$ – droplet velocity vector, $\mathrm{m/s}$;
X – local bulk mole fraction of moisture;
Y_d – mass fraction of droplets with diameter greater than d_p;
α – spread parameter for the Rosin-Rammler distribution function;
σ – surface tension, $\mathrm{N/m}$;
ρ_l – liquid density, $\mathrm{kg/m^3}$;
η – liquid viscosity, $\mathrm{kg/(m \cdot s)}$;
ρ – droplet density, $\mathrm{kg/m^3}$;
ρ_g – gas density, $\mathrm{kg/m^3}$;
τ – stress tensor, $\mathrm{N/m^2}$;
μ – viscosity, $\mathrm{kg/(m \cdot s)}$;
ε – energy dissipation rate, $\mathrm{m^2/s^3}$;
σ_k – turbulent Prandtl number for k;
σ_ε – turbulent Prandtl number for ε;
μ_t – turbulent viscosity.

Non-dimensional number

Re – Reynolds number $\left(\mathrm{Re} = \dfrac{\rho d_p \left|\overrightarrow{u_g} - \overrightarrow{u_p}\right|}{\mu}\right)$;

Nu_{AB} – Nusselt number $\left(\dfrac{k_c d_p}{D_m}\right)$;

Nu – Nusselt number $\left(\dfrac{h d_p}{k_\infty}\right)$;

Sc – Schmidt number $\left(\dfrac{\mu}{\rho D_m}\right)$;

Pr – Prandtl number of gas ($c_p \mu / k_g$).

Subscripts

g – air;
p – droplet;
l – liquid;
eff – effective.

Introduction

Spray drying consists of four process stages, i.e., atomization of feed into a spray; hot-air generation system; spray evaporation or drying via spray and hot air contact; and separation of dried products from the exhaust air. The atomization of feed plays a very important role in spray drying [Filkova and Mujumdar, 1995]. In particular, successful selection and operation of the atomizer can lead to economic production of high quality products of desired properties [Masters, 1991]. There are two basic types of atomizer, i.e., rotary/centrifugal atomizer and nozzles. The commonly used nozzles are pressure nozzle and pneumatic nozzle (two-fluid or three-fluid nozzle). Pneumatic nozzle is less used due to its high energy consumption. Pressure nozzles are generally used to form

coarse powders (mean size 120-300 μm). The ultrasonic nozzle provides advantages because of its smaller droplet size, relatively uniform size distribution, relatively large permissible liquid flow rates and low liquid feed pressure [Rajan and Pandit, 2001]. Recently, Bittner and Kissel [1999] studied use of the ultrasonic nozzle in a conventional spray dryer to produce protein-loaded microspheres from poly (lactide-co-glycolide). They showed that the ultrasonic nozzle can be an alternate atomization device which can be used in a spray dryer.

Since the computational fluid dynamics technique has developed very rapidly over the past decades, many authors have developed CFD models to simulate high-temperature and low-temperature co-current spray dryers with reasonable success [Crowe, Sommerfeld and Tsuji, 1998; Ducept, Sionneau and Vasseur, 2002; Huang, Kumar and Mujumdar, 2003a and 2003b; Kieviet, 1997; Langrish and Keckel, 2001; Langrish and Zibincinski, 1994; Levi-Hevroni, Levy and Borda, 1995; Southwell and Langrish, 2000; Wu and Liu, 2002]. Although the complex transport phenomena occurring in a spray dryer cannot yet be modeled with high accuracy, the results are nevertheless useful to guide design and operation of spray dryers when coupled with empirical experience.

In this study, a CFD simulation [FLUENT 6.0] was carried out to predict the spray evaporation performance in a co-current cylinder-on-cone spray chamber. The correlation developed by Rajan and Pandit [2001] which accounts for the physico-chemical properties of the liquid as well as the ultrasonic properties of the atomizer (amplitude, frequency, area of vibrating surface) was used to predict the performance of the ultrasonic nozzle. The correlation is proposed as follows

$$d_p = \text{const}\, a\ nt(f)^{-0.66}(Q)^{0.207}(\sigma)^{0.11}(\rho)^{-0.274}(\eta)^{0.166}(\text{power}/\text{area})^{-0.4}\ . \quad (1)$$

Two types of atomizers, e.g., ultrasonic atomizer and pressure nozzle, are selected in this paper for a comparative evaluation. The predicted results with ultrasonic atomizer for spray evaporation performance are compared with those for a conventional pressure atomizer in the same dryer configuration and using identical parameter values except for the droplet size and its distribution at the nozzle. The advantages and limitations of using an ultrasonic atomizer rather than the conventional one are discussed in the light of the simulation results. It should be noted that the simulations are for evaporation of water droplets rather than for drying of solutions or suspensions.

PHYSICAL MODEL

Geometric configuration of the chamber

Figure 1 shows the tested spray dryer geometry which is the same as that studied by Kieviet [1997] and Huang et al. [2003 b]. This chamber is a cylinder-on-cone vessel, 2.215 m in diameter, cylindrical top section, 2.0 m high with a bottom cone 1.725 m high. The angle of the bottom cone is 60°.

Governing equations for simulation

The flow in a spray dryer is turbulent and two-phase (gas and droplets or gas and particles). Hence, we employed a flow model in which one of the phases (droplets or particles) is dispersed throughout the other phase (gas or air). Two-way coupling is assumed between the two phases, i.e., there is finite transfer of momentum, heat and mass between the two phases which affect the transfer processes in each phase. We use Eulerian-Lagrangian method to model the two-phase flow.

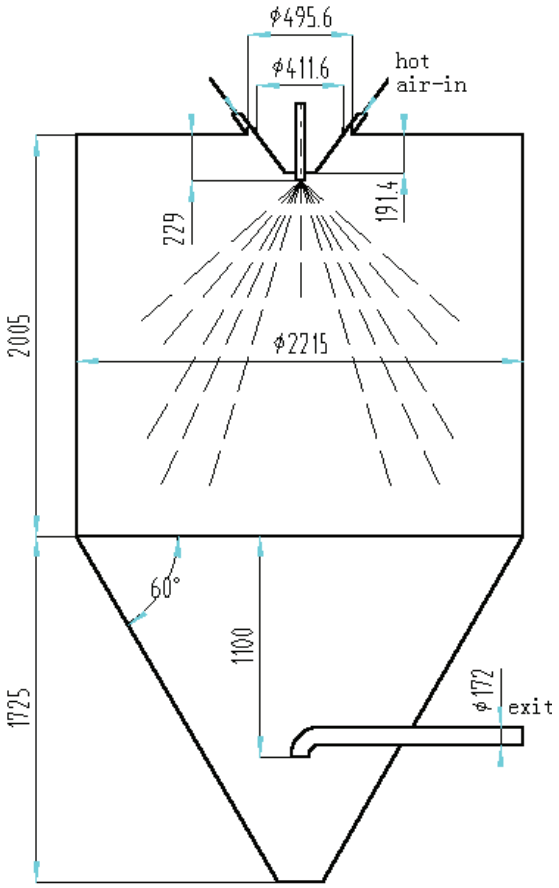

Fig. 1 Physical geometry (All dimension in mm) (Kieviet, 1997)

- ***Governing equations for the gas-phase/***

The continuity equation is [Bird, Stewart and Lightfoot, 1960; Ferziger & Peric, 1999]

$$\frac{\partial \rho_g}{\partial t} + \nabla \bullet (\rho_g \overrightarrow{u_g}) = M_m, \tag{2}$$

with fluid density ρ_g, time t, coordinate and velocity $\overrightarrow{u_g}$ and source term M_m, which accounts for any mass addition or user-defined source.

Momentum equations

$$\frac{\partial (\rho_g u_g)}{\partial t} + \nabla \bullet \left(\rho_g \overrightarrow{u_g}\overrightarrow{u_g}\right) = -\nabla P + \nabla \bullet \tau + \rho_g \vec{g} + \overrightarrow{M_F}. \tag{3}$$

It is in accordance with Newton's law. The last term $\overrightarrow{M_F}$ is the source term or external body force, e.g., interaction forces of a dispersed phase (particles) on the continuous phase (fluid). The two-dimensional axi-symmetrical form of equation (3) is used for the present simulations.

For Newtonian fluids, the components of the stress tensor τ_{ij} in eq.(3) can be written as

$$\tau_{ij} = \mu\left(\frac{\partial u_i}{\partial x_j} + \frac{\partial u_j}{\partial x_i}\right) - \frac{2}{3}\delta_{ij}\frac{\partial u_1}{\partial x_1}, \quad (4)$$

with the fluid viscosity μ and the volume dilation term with the 'Kronecker' delta

$$\delta_{ij} = \begin{cases} 1 \text{ for } i = j; \\ 0 \text{ for } i \neq j. \end{cases} \quad (5)$$

Energy equation

$$\frac{\partial}{\partial t}(\rho_g E) + \nabla \bullet \left(\vec{u}(\rho_g E + P)\right) = \nabla \bullet \left(k_{\text{eff}} \nabla T - \sum_j H_j \vec{J}_j + (\overline{\tau_{\text{eff}}} \bullet \vec{u})\right) + M_h. \quad (6)$$

The source term M_h is the heat transfer per unit volume between dispersed and continuous phases.

- ***Governing equations for dispersed phase (particle or droplet)***

(1) Droplet trajectories

The particle trajectories are obtained by solving the force balance for the particles by considering the discrete phase inertia, aerodynamic drag, gravity $\vec{g}$ and further optional user-defined forces $\vec{F}$.

$$\frac{d\overrightarrow{u_p}}{dt} = C_D \frac{18\mu}{\rho_p d_p}\frac{\text{Re}}{24}\left(\overrightarrow{u_g} - \overrightarrow{u_p}\right) + \vec{g}\frac{\rho_g - \rho}{\rho_g} + \vec{F}. \quad (7)$$

The relative Reynolds number is defined as

$$\text{Re} = \frac{\rho d_p \left|\overrightarrow{u_g} - \overrightarrow{u_p}\right|}{\mu} \quad (8)$$

and drag coefficient which is a function of the particle Reynolds number is given by

$$C_D = a_1 + \frac{a_2}{\text{Re}} + \frac{a_3}{\text{Re}^2}, \quad (9)$$

where a_1, a_2 and a_3 are empirically fitted constants [Morsi and Alexander, 1972].

(2) Mass transfer between droplets and gas

For spray water, the rate of vaporization is governed by concentration gradient diffusion between droplet surface and gas phase, i.e.,

$$N_i = k_c (C_s - C_g), \quad (10)$$

where N_i – molar flux of vapor mol/(m^2·s); k_c – mass transfer coefficient (m/s); C_s – vapor concentration at the droplet surface, kmol/m^3; C_g – vapor concentration in the bulk gas phase, mol/m^3; C_s and C_g are given by

$$C_s = \frac{p_{\text{sat}}(T_p)}{RT_p}; \quad (11)$$

$$C_g = X \frac{p_{\text{op}}}{RT_\infty}. \tag{12}$$

The mass transfer coefficient in equation (10) is calculated using analogy between heat and mass transfer from the classical Nusselt number correlation [Ranz and Marshal, 1952, Part I & II]

$$\text{Nu}_{AB} = \frac{k_c d_p}{D_m} = 2.0 + 0.6\,\text{Re}^{1/2}\,\text{Sc}^{1/3}. \tag{13}$$

The mass of droplet is reduced due to evaporation according to

$$\Delta m_p = N_i A_p M_w \Delta t. \tag{14}$$

(3) Heat transfer between the droplets and gas

The heat transfer between the droplet and the hot gas is updated after each time step according to the heat balance as follows

$$m_p c_p \frac{dT_p}{dt} = hA_p \left(T_g - T_p\right) + \frac{dm_p}{dt} h_{fg}. \tag{15}$$

The heat transfer coefficient, h, is evaluated using the correlation of Ranz and Marshall [1952, Part I & II]

$$\text{Nu} = \frac{hd_p}{k_g} = 2.0 + 0.6\,\text{Re}^{1/2}\,\text{Pr}^{1/3}. \tag{16}$$

- ***Coupling between dispersed and continuous phase***

Since Fluent uses a finite-volume method to simulate the two phase flow, the two-way coupling is computed in every controlled volume. In each computation time step Δt, the two-way coupling between dispersed and continuous phase is computed as follows [Fluent Inc., 2002]

(1) Momentum exchange

The momentum transfer from the continuous phase to the dispersed phase in the controlled volume is computed by

$$M_F = \sum \left(\frac{18\mu C_D \,\text{Re}}{24\rho_p d_p^2} (u_p - u) + F_{\text{other}} \right) \dot{m}_p \Delta t, \tag{17}$$

where u_p is the velocity of the particle, u is the velocity of the fluid, C_D is drag coefficient, $\dot{m}_p$ is mass flow rate of the particles in the controlled volume, Δt is time step, F_{other} is other interaction forces.

(2) Heat transfer between the dispersed and the continuous phase

Heat transfer from the continuous phase to the discrete phase is computed in Fluent 6.0 [2002] as

$$M_h = \left[\frac{\bar{m}_p}{m_{p,0}} c_p \Delta T_p + \frac{\Delta m_p}{m_{p,0}} \left(-h_{fg} + \int_{T_{ref}}^{T_p} c_{p,i}\, dT \right) \right], \tag{18}$$

where $\bar{m}_p$ is average mass of the particle in the control volume, kg, $m_{p,0}$ is initial mass of the particle, kg, c_p is heat capacity of the particle, J/(kg·K), ΔT_p is temperature change of the particle in the control volume, K, Δm_p is change of the mass of the particle in the control volume, kg, h_{fg} is latent heat of volatiles evolved, J/kg, $c_{p,i}$ is heat capacity of the volatiles evolved, J/(kg·K), T_p is temperature of the particle upon exit of the control volume, K, T_{ref} is reference temperature for enthalpy, K, $\dot{m}_{p,0}$ is initial mass flow rate of the particle injection tracked, kg/s. It appears as a source or sink of energy in the continuous phase energy balance.

(3) Mass transfer between the dispersed and the continuous phase

Mass transfer from the discrete phase to the continuous phase in the controlled volume is computed simply as

$$M_m = \frac{\Delta m_p}{m_{p,0}} \dot{m}_{p,0} \ . \tag{19}$$

This appears as a source of mass in the continuous phase continuity equation.

- ***Turbulence model***

Gas flow in spray drying is usually turbulent. Oakley [1992] showed that standard *k*-epsilon model may be used to simulate the turbulent flow in spray dryer when gas flow at inlet has small swirling component. Other turbulence models are also available but from the viewpoint of computational economy tests were made only with the k-ε model.

Two additional transport equations have to be solved in the k-ε model, one equation for the turbulent kinetic energy k, and another equation for the turbulence dissipation rate ε. They are

$$\frac{\partial}{\partial t}(\rho k) + \frac{\partial}{\partial x_i}(\rho u_i k) = \frac{\partial}{\partial x_i}\left[\left(\mu + \frac{\mu_t}{\sigma_k}\right)\frac{\partial k}{\partial x_i}\right] + G_k + G_b - \rho\varepsilon - Y_M + S_k \tag{20}$$

and

$$\frac{\partial}{\partial t}(\rho\varepsilon) + \frac{\partial}{\partial x_i}(\rho u_i \varepsilon) = \frac{\partial}{\partial x_i}\left[\left(\mu + \frac{\mu_t}{\sigma_\varepsilon}\right)\frac{\partial \varepsilon}{\partial x_i}\right] + B_1 \frac{\varepsilon}{k}(G_k + B_3 G_b) - B_2 \rho \frac{\varepsilon^2}{k} + S_\varepsilon . \tag{21}$$

The five empirical parameters, i.e., B_1, B_2, B_3, σ_k and σ_ε, are given by Launder and Spalding [1972 and 1974]. The viscosity μ is computed as

$$\mu = \mu_{\text{eff}} + \mu_t \ . \tag{22}$$

The turbulent viscosity μ_t is defined as

$$\mu_t = \rho c_\mu \frac{k^2}{\varepsilon} \ . \tag{23}$$

Boundary conditions

The simulations are performed for steady state operation. The grid-independence of the results has been shown in a previous paper [Huang et al., 2003b].

The boundary conditions are defined at the inlet, the outlet, chamber wall and the turbulence model. We summarize them in Table 1.

Table 1

Boundary conditions used for simulation

Air mass flow rate, kg/s	Air temperature, °C	Air absolute Humidity, kg/kg	Spray rate, kg/s	Rosin-Rammler parameter	Feed temperature, °C
0.336	195	0.0101	0.0111111	2.05	27

Air radial velocity, m/s	Air axial velocity, m/s	Air total velocity, m/s	Turbulence k-value, m^2/s^2	Turbulence ε -value, m^2/s^3	Pressure at outlet, Pa
-5.252	7.488	9.146	0.027	0.37	0/-1000.0

Chamber wall thickness, m	Wall material	Wall heat transfer coefficient, $W/m^2 \cdot K$	Air temperature outside wall, °C	Interaction B.C. between wall and droplet
0.002	Steel	3.5	27	Escape

• Inlet air: The drying air flow rate is 0.336 kg/s. Temperature of air at inlet is set at 468 K and its relative humidity is 75 % at 25 °C.

• Outlet conditions: The outlet pressure is set at 0 Pa or –1000 Pa for different test cases. In practice, this pressure is maintained at a slight negative value.

• Chamber wall conditions: When a droplet/particle hits the wall of the drying chamber, we assume that the droplets "escape" via the wall. Under the "escape" condition, the particles are lost from the calculation domain at the point of impact with the wall. The overall heat transfer coefficient from the wall to the outside of the drying chamber is estimated to be 3.5 $W/(m^2 \cdot K)$ while the chamber wall is assumed to be made of stainless steel, 2mm thick. This coefficient value is obtained by fitting published measured data [Kieviet, 1997] with a simulation carried out with spray. It is slightly higher than that observed in normal spray dryers [Masters, 2002].

• Spray from nozzle: The main difference from the results of Huang et al. [2003b] is the atomization type (pressure nozzle versus ultrasonic nozzle) and droplet size distribution. We still use a Rosin-Rammler distribution with a spread parameter equal to 2.05 [Kieviet, 1997] to model the droplet size distribution. This function is given by [Masters, 1991]

$$Y_d = 100 e^{\left(-\frac{d_p}{\bar{d}}\right)^{\alpha}}. \qquad (24)$$

The spray mass flow rate is 40 kg/h (0.011111 kg/s). The feed temperature is set at 300 K. Feed is pure water. The initial droplet velocity and droplet size distribution are different for test cases shown in Table 2.

• Turbulence model: For this 2D-axisymmetric model, the normal k-ε turbulence model, the RNG k-ε model, the realizable k-ε model and the Reynolds stress model (**RSM**) were used to compare the simulated results. As expected the predicted results are dependent on the turbulence model and for each turbulence model the grid design for grid-independence depends on the model as well. The predicted results by the standard k-ε turbulence model agreed well with the experimental data of Kieviet [1997]. This favorable comparison has been reported previously by Huang et al. [2003b]. Hence the standard k-ε turbulence model is used in this study. Another reason for its use is that the k-ε model [Launder et al., 1974] is expected to be a reasonable choice for simulating such a flow [Oakley et al., 1992], because there is no swirl in the drying chamber.

Table 2

Cases studied in simulation

Cases	Droplet size distribution, μ*m*	Mean droplet size, μ*m*	Droplet velocity of *x*, m/s	Droplet velocity of *y*, m/s	Total droplet velocity, m/s
1	1.0…20.0	10.0	0.01	0.01	0.014
2			5.5	1.0	5.59
3			46.49	36.32	59.0
4	20.0…40.0	30.0	0.01	0.01	0.014
5			5.5	1.0	5.59
6			46.49	36.32	59.0
7	40.0…60.0	50.0	0.01	0.01	0.014
8			5.5	1.0	5.59
9			46.49	36.32	59.0
10	60.0…80.0	70.0	0.01	0.01	0.014
11			5.5	1.0	5.59
12			46.49	36.32	59.0
13	80.0…100.0	90.0	0.01	0.01	0.014
14			5.5	1.0	5.59
15			46.49	36.32	59.0
16	100.0…120.0	110.0	0.01	0.01	0.014
17			5.5	1.0	5.59
18			46.49	36.32	59.0
19	10.0…250.0	150.0	0.01	0.01	0.014
20			5.5	1.0	5.59
21			46.49	36.32	59.0
22	10.0…120.0	60.0	0.01	0.01	0.014
23			5.5	1.0	5.59
24			46.49	36.32	59.0
25	1.0…60.0	30.0	0.01	0.01	0.014
26			5.5	1.0	5.59
27			46.49	36.32	59.0

The turbulent kinetic energy at the inlet was set at 0.027 m^2/s^2, and the energy dissipation rate at the inlet at 0.37 m^2/s^3, which are the same values as those used by Kieviet [1997] and Huang et al. [2003b]. For tracking the droplets, the turbulent stochastic model (**TSM**) option was used. Turbulent stochastic tracking of droplets admits the effect of random velocity fluctuations of turbulence on particle dispersion to be accounted for in the prediction of the particle trajectories. For details the readers may refer to Fluent 6.0 manual [Fluent, 2002]

Results and discussion

We compare the predicted velocity at the no spray condition and temperature profiles at spray condition along with the measured results by Kieviet [1997] at different levels in the drying chamber in Figure 2 and 3, respectively. The simulation boundary conditions are followed to Kieviet [1997] and discussed in details by Huang et al. [2003b]. These Figures show that our predicted velocities agree well with the measured results.

In Fig. 2, we see that there is a non-uniform velocity distribution in the core region of the chamber. The highest velocity magnitude is about 7.0 m/s at the 0.30 m level.

In Fig. 3, the simulation results provide details of the temperature field at different levels. The measurement results do not give such detail because of the small number of measurement points. From the predicted temperature profile, we find that the temperatures in the central core of diameter of about 0.25 m are quite different at

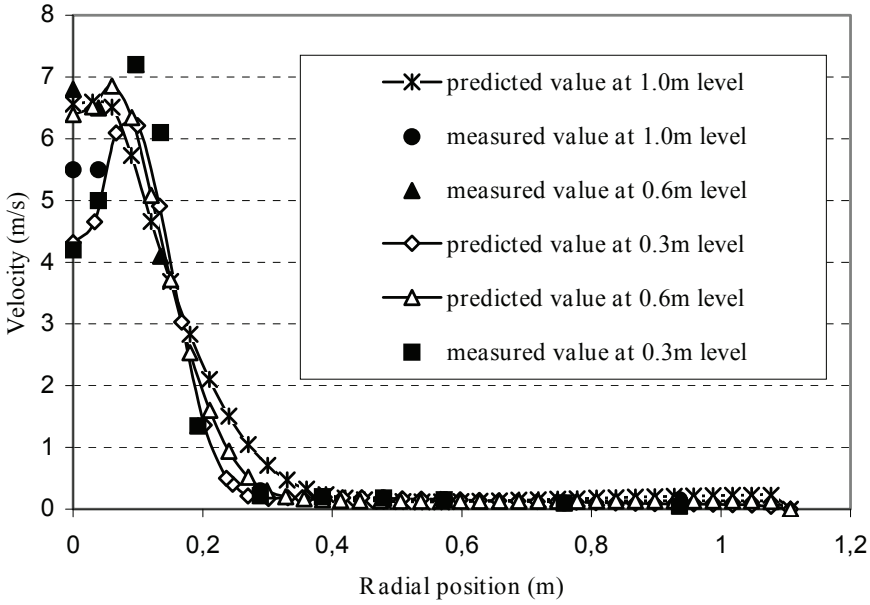

Fig. 2 Comparison of velocities at different levels measured from the ceiling (0.3 m, 0.6 m, 1.0 m and 1.4 m) in the drying chamber between predicted results and measured results [Kieviet, 1997]

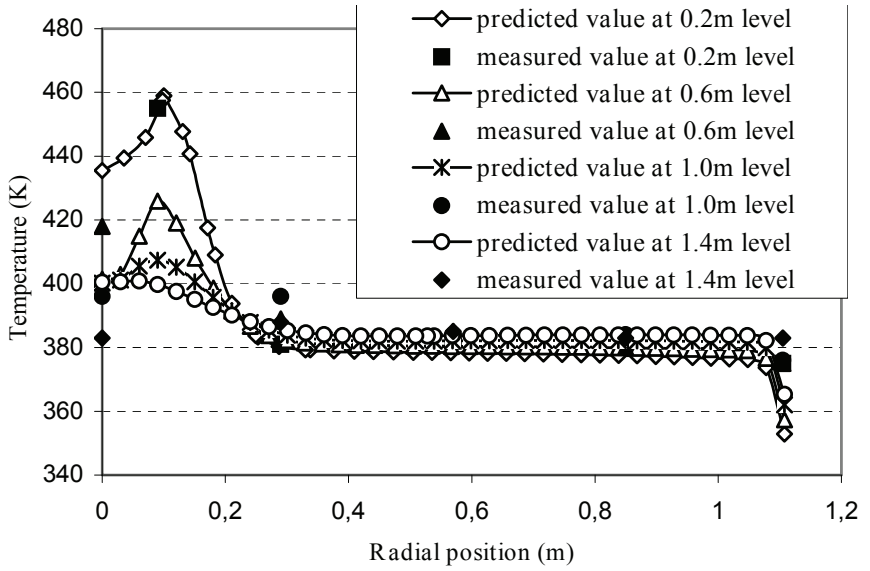

Fig. 3 Comparison of temperatures at different levels measured from the ceiling (0.2 m, 0.6 m, 1.0 m and 1.4 m) in the drying chamber between predicted results and measured results [Kieviet, 1997]

different levels; this is expected as a direct result of drying. There is only a minor radial variation in the gas temperature. The largest temperature changes usually occur at the first level. It is a result of the very high heat and mass transfer rates in the nozzle zone due to high relative velocities between the gas and the droplets coupled with large temperature driving forces.

Based on the geometric and grid conditions, we defined the test cases which are simulated with droplet size distribution and initial velocity listed in Table 2. We used different droplet size distributions, e.g., 1.0 to 20 μm ; 20 to 40 μm ; 40 to 60 μm ; 60 to 80 μm ; 80 to 100 μm ; 100-120 μm ; 1.0 to 60 μm ; 10 to 120 μm and 10 to 250 μm . Due to the low initial velocity of droplets issuing from an ultrasonic atomizer, we used three different relatively low initial droplet velocities, i.e., 0.01 m/s as static droplet; 5.59 m/s as representative values for ultrasonic atomizers [Rajan and Pandit, 2001], and 59 m/s as that for the pressure nozzle [Kieviet, 1997 and Huang et al., 2003b].

Some of the simulation results, e.g., air velocity, temperature and humidity profiles in the chamber have been reported earlier for pressure nozzle [Huang, Kumar and Mujumdar, 2003b]. With ultrasonic nozzles, these do not change significantly, and hence they are not reported here.

Due to limited space, Figure 4 only provides the particle trajectories for selected cases viz. cases 16, 17, 18, 25, 26 and 27. We find that the particle trajectory profiles are only slightly different for Cases 16, 17, 25 and 26, i.e., the small initial droplet velocity does not influence the particle trajectories significantly. When the droplet velocity is high, such as, in atomization from pressure nozzles, we find the particles begin to occupy all of the volume of the drying chamber. The high inertia droplets are able to reach the re-circulation region and there some of droplets are lifted by the upward air flow. We also find that many particles hit the conical wall regardless of the initial droplet velocity or droplet size distribution. For small mean droplet sizes, such as, cases 1, 2, 3, 4, 5 and 6, the droplets only travel a short distance before they disappear due to their small mass and less time. required complete evaporation.

We provide the number of droplets with different “fates” viz. evaporation, trap and escape, for all test cases in Table 3. The “evaporation fate” means that the droplets are completely evaporated before they hit the wall or reach the outlet. “Trapped” droplets report the number of droplets that finally hit the wall. In the simulation process, the computation of evaporation is stopped. “Escape” fate for the droplets means that the droplets reach the chamber outlet and leave the outlet with exhaust air. At the same time, the computation for these droplets is stopped as well.

From Table 3, we find that the number of droplets with “evaporation fate” are greater when the initial droplet velocity is 0.01m/s and 59 m/s and the maximum droplet diameter is less than 60 μm than that when the initial droplet velocity is 5.59 m/s and the same droplet size distribution is used. The reason for this observation is that the air velocity is about 7 m/s [Huang et al., 2003b] in the central zone, which is almost the same as the droplet velocity, i.e., 5.59 m/s, when the droplets are just sprayed from the atomizer. The low relative velocity between the droplet and the air leads to reduced mass transfer rate from the droplets. On the other hand, when the droplet size is between 60 μm and 120 μm , such as, in cases 10,11,12,13,14,16 etc., the results differ from the above conclusion. The number for evaporated droplets for the ultrasonic atomizer is greater than those from static droplets or droplets issuing from the pressure nozzle.

Finally, we simulated the cases with the normal droplet size distribution for cases 19 through 27. We find that the cases with smaller mean droplet diameter have a greater number of evaporated droplets. This is expected as the smaller size droplets need less evaporation time. So if the traveling distance is sufficient before they reach the wall or outlet, the droplets are fully evaporated.

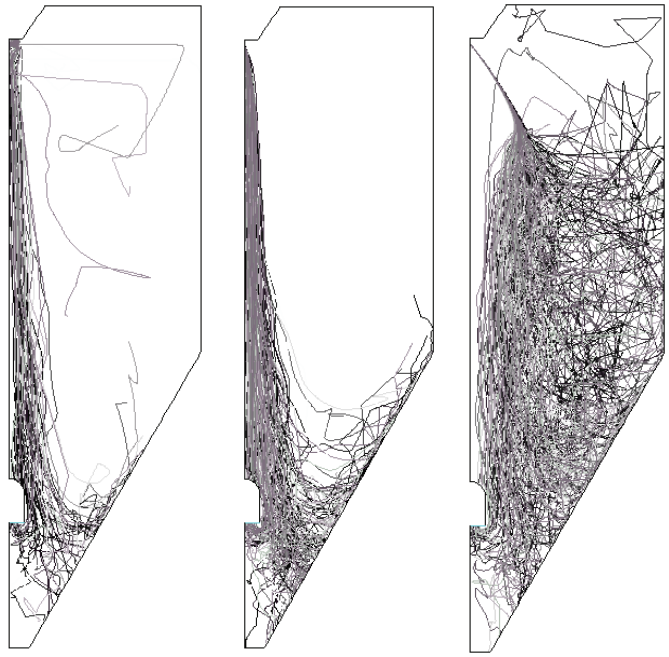

(*a*) *Case 16* (*b*) *Case 17* (*c*) *Case 18*

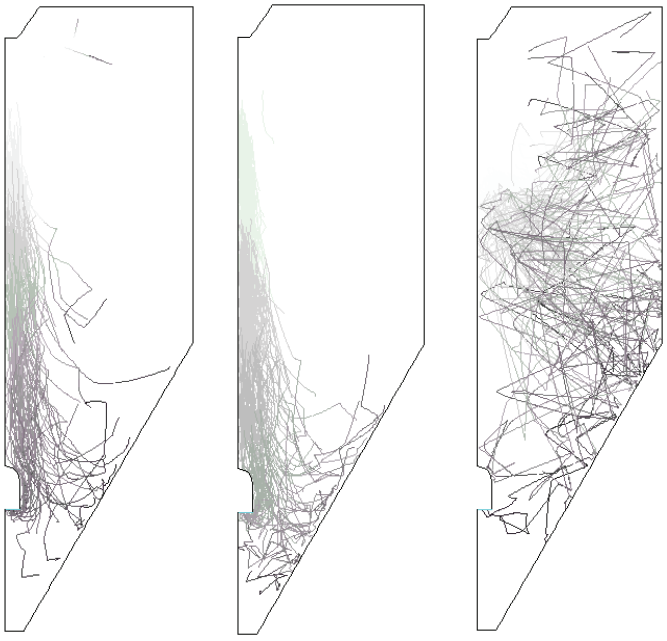

(*a*) *Case 25* (*b*) *Case 26* (*c*) *Case 27*

Fig. 4 Particle trajectories for cases 16, 17, 18, 25, 26 and 27

In Table 3, we provide the mean residence time for the droplets for evaporation, trapped at the wall and escaping from the outlet as well. The droplets that escape from the outlet usually have longer residence times than those that are fully evaporated or trapped at the wall. It is because the particles for evaporation and being trapped at the wall usually travel a short distance. On the other hand, we find that the mean residence time becomes longer when the mean droplet diameter increases.

Table 3

Particle residence time in the drying chamber for the test cases

Cases	Evaporated droplet		Trapped droplet		Escaped droplet	
	Number	Mean residence time, s	Number	Mean residence time, s	Number	Mean residence time, s
1	184	0.122	16	0.103		
2	141	0.0448	69	0.0454		
3	192	0.0815	8	0.0621		
4	139	0.319	54	0.0627	7	0.5864
5	186	0.3205	5	0.4146	9	0.4922
6	150	0.4586	10	0.4817	40	0.484
7	199	0.0173	1	0.0397		
8	121	0.9229	30	0.767	49	0.5846
9	117	1.501	43	1.731	40	0.6939
10	55	1.179	111	0.215	34	0.6406
11	86	1.358	42	1.117	72	0.6156
12	52	3.21	104	2.286	44	1.15
13	14	0.7576	171	0.06	15	0.5527
14	40	1.66	89	1.056	71	0.6734
15	26	5.353	134	2.525	40	1.575
16	12	2.138	167	0.3078	21	0.6892
17	19	2.124	100	0.868	81	0.628
18	14	7.027	153	2.615	33	1.856
19	36	0.6539	141	0.5457	23	0.674
20	47	0.4445	114	0.707	39	0.5987
21	75	1.457	116	1.982	8	1.204
22	92	0.6242	74	0.3554	34	0.7174
23	95	0.7145	52	0.8615	53	0.5841
24	97	0.8501	72	2.535	31	1.773
25	136	0.3916	47	0.1263	17	0.7055
26	154	0.3302	14	0.5285	32	0.6416
27	175	0.8139	24	1.606	1	2.23

In Table 4, we summarize the evaporation performance, such as, evaporation rate, unit heat consumption per unit evaporation rate and percentage of evaporation etc., for all cases. We find that the evaporation rate and percentage of evaporation are high when the maximum droplet diameter is less than $60\,\mu m$. Higher evaporation rate make the unit energy consumption per unit evaporation lower.

Table 4

Predicted overall evaporation performance for the test cases

Cases	Evaporation rate, kg/s	Energy consumption for evaporation, kJ/s	Heat loss from wall (kJ/s)	Unit energy consumption / unit evaporation rate, kJ/kg	Evaporation percent, %
1	0.0106	24.067	4.945	2737	95.4
2	0.0089	20.697	6.243	3027	80.1
3	0.01107	24.98	6.032	2801	99.6
4	0.008515	19.101	5.331	2869.3	76.64
5	0.01106	24.954	5.791	3051	99.54
6	0.0107032	24.27	5.08	2742	99.33
7	0.1088	25.009	6.715	2915	97.92
8	0.010	22.897	5.388	2818.5	90.0
9	0.0107	24.23	5.005	2732	96.3
10	0.00521	12.332	6.067	3531	46.89
11	0.0093655	21.649	5.659	2915	84.29
12	0.0095265	21.967	5.152	2947	85.74
13	0.00182	4.7738	6.986	6461	16.38
14	0.007928	18.851	5.966	3130	71.35
15	0.00761	18.237	5.286	3091	68.49
16	0.00246	6.117	6.564	5155	22.14
17	0.0065131	16.095	6.372	3449.5	58.61
18	0.00586	16.875	5.613	3837	52.74
19	0.004263	10.632	7.215	4186.5	38.37
20	0.005591	14.294	6.569	3731.5	50.32
21	0.007254	17.537	5.842	3223	65.286
22	0.008087	18.485	5.818	3005.2	72.78
23	0.009081	21.106	5.665	2948	81.73
24	0.009984	22.86	5.185	2808	89.86
25	0.008992	20.306	5.535	2874	80.9
26	0.01073	24.324	5.56	2785	96.57
27	0.01103	24.912	5.884	2792	99.27

When the droplet diameter increases from 60 μm and a narrow size distribution is used, the evaporation percentage shows that spray drying with ultrasonic atomizer has a better drying performance.

On the other hand, no matter which type of atomizer is used to atomize the feed, the high evaporation rate still can be obtained if the maximum droplet diameter is less than 60 μm and the large range of droplet size distribution is used. However, when the

maximum droplet diameter greater than $60\,\mu m$ and the large droplet size distribution are used, the cases, i.e., cases 21, 24 and 27, with pressure nozzle have the best evaporation performance among the three droplet initial velocities. Ultrasonic atomizer also can be used if it is able to produce such a droplet size distribution.

From Table 4, we find that heat loss from the chamber wall is different because the wall temperature is different due to different air temperature near the wall by the varied evaporation rate. Higher wall temperature leads to higher heat loss from the wall. In this simulation, greater heat loss from the wall is due to larger heat transfer coefficient used in simulation. Another reason is that not all water is evaporated finally in some cases, such as, Cases 2, 16 and 19 etc. It directly results in higher outlet and wall temperatures.

From the above mentioned results in Table 4, we find that the ultrasonic atomizer does not give a better evaporation performance than the pressure nozzle does. We also can see that the bulk density will be smaller if the ultrasonic atomizer is used in spray dryer due to the narrow particle size distribution. But for special cases, e.g., mono-sized particle product, we may consider selection of the ultrasonic atomizer for spray drying.

Conclusions

A computational fluid dynamics model was used to simulate spray drying with ultrasonic atomizer and pressure nozzle. Different size distribution of droplet and initial velocity are used in simulation cases. The predicted results for spray evaporation of water in a cylinder-on-cone chamber are presented and compared with the literature data. Good agreements between predictions and experimental data are obtained. The predicted results show that ultrasonic atomizer can be used in spray drying for special applications requiring nearly mono-sized particles.

The predicted results for the cases with narrow and large range of droplet size distribution and for different initial droplet velocities are discussed. Spray drying with droplet diameters greater than $60\,\mu m$ and the ultrasonic atomizer, e.g., with a narrow droplet size distribution, has a better evaporation performance than those with static droplets and pressure nozzle. For large range of droplet size distribution, the spray drying with pressure nozzle still shows best drying performance among the three types of initial droplet velocities. It is due to large relative velocity between drying medium and droplet and longer residence time before they hit the wall or reach the outlet. The main advantage of the ultrasonic atomizer is in being able to produce smaller, mono-size powders rather than in avoiding wall deposits or enhancing dryer thermal performance.

References

1. Bird, R.B., Stewart, W.E. and Lightfoot, E.N., 1960, Transport Phenomena, John Wiley & Sons Inc., New York, Pp. 273.

2. Bittner, B. and Kissel, T., 1999, Ultrasonic atomization for spray drying: a versatile technique for the preparation of protein loaded biodegradable microspheres, Journal of Microencapsulization, 16 (3), Pp. 325 – 341.

3. Crowe, C.; Sommerfeld, M. and Tsuji, Y. (1998), Multiphase Flows with Droplets and Particles (60-65); Boca Raton, Fla.: CRC Press.

4. Ducept, F.; Sionneau, M. and Vasseur, J. (2002), Superheated Steam Dryer: Simulations and Experiments on Product Drying; Chem. Eng. J.; 86, Pp. 75 – 83.

5. Ferziger, J.H. and Meric, M., 1999, Computational Methods for Fluid Dynamics, 2nd Ed., Berlin; New York; Springer, Pp. 375.

6. Filkova I. and Mujumdar A.S. (1995); Industrial Spray Drying Systems; in Mujumdar A.S. (Eds.), Handbook of Industrial Drying (2nd Ed. pp.263-308), Marcel Dekker, Inc.: New York, 1.

7. Fluent Manual (2002); chap. 19: Discrete Phase Models; www.fluent.com.

8. Huang, L., Kumar, K. And Mujumdar, A.S. (2003a), Use of Computational Fluid Dynamics to Evaluate Alternative Spray Chamber Configurations, Drying Technology, 21(3), Pp. 385 – 412.

9. Huang, L, Kumar, k and Mujumdar, A.S., (2003b), A Parametric Study of the Gas Flow Patterns and Drying Performance of Co-current Spray Dryer: Results of a Computational Fluid Dynamics Study, Drying Technology, 21 (6), (In Press).

10. Kieviet, F.G (1997), Modelling Quality in Spray Drying, PhD thesis, Endinhoven University of Technology, the Netherlands.

11. Langrish, T.A.G. and Zbincinski, I. (1994), The Effects of Air Inlet Geometry and Spray Cone Angle on the Wall Deposition Rate in Spray Dryers; Trans. I. Chem. E., 72(A), Pp. 20 – 430.

12. Langrish, T.A.G. and Kockel, T.K. (2001), the Assessment of a Characteristic Drying Curve for Milk Powder for Use in Computational Fluid Dynamics Modelling; Chem. Eng. J.; 84, Pp. 69 – 74.

13. Launder, B.E. and Spalding, D.B., 1972, Lectures in mathematical models of turbulence, Academic press, London, England.

14. Launder, B.E. and Spalding, D.B., 1974, The Numerical Computation of Turbulent Flows; Comput. Methods Appl. Mech. Eng.; 3 Pp. 269 – 289.

15. Levi-Hevroni, D.; Levy, A. and Borde, I. (1995), Mathematical Modelling of Drying of Liquid/Solid Slurries in Steady State One-Dimensional Flow; Drying Technology; 13(5-7), Pp. 1187 – 1201.

16. Masters, K., 1991, Spray Drying Handbook, Longman Scientific & Technical and John Wiley & Sons, Inc., New York, 725 pp.

17. Morsi, S.A. and Alexander, A.J., 1972, An investigation of particle trajectories in two-phase flow systems, J. Fluid Mech., 55(2), Pp. 193 – 208.

18. Oakley, D.; Bahu, R. and Reay, D., 1992, The Aerodynamics of Co-current Spray Dryers; in DRYING'92; Mujumdar, A.S. Ed.; Elsevier : Amsterdam; pp.359-364

19. R. Rajan and A. B. Pandit, 2001, Correlations to predict droplet size in ultrasonic atomisation, Ultrasonics, 39(4), Pp. 235 – 255.

20. Ranz, W.E. and Marshall, W.R. Jr., 1952, Evaporation from drops, Part I, Chemical Engineering Progress, 48(3), Pp. 141 – 146.

21. Ranz, W.E. and Marshall, W.R. Jr., 1952, Evaporation from drops, Part II, Chemical Engineering Progress, 48(4), Pp. 173 – 180.

22. Southwell, D.B. and Langrish, T.A.G. (2000), Observations of Flow Patterns in a Spray Dryer; Drying Technology; 18 (2), 661 – 685.

23. Wu, Z.H. and Liu, X.D. (2002), Simulation of Spray Drying of a Solution Atomized in a Pulsating Flow; Drying Technology; 20 (6), 1101 – 1121.

Моделирование распылительной сушки при использовании механического и ультразвукового распылителей – сопоставительный анализ

Хуанг Ликсин[1], К. Кумар[2], Арун С. Муджумдар[1]

Кафедра механических процессов,
Национальный университет Сингапура (1)
Отделение вычислительной гидродинамики,
Институт высокоточных вычислений (2)

Ключевые слова и фразы: вычислительная гидродинамика; распределение капель по размерам; сопло; сушка распылением.

Аннотация: Обычное механическое распыление сообщает высокую начальную скорость каплям, что приводит к большому разбросу капель по размерам. Если струя создается при помощи ультразвуковой энергии, то можно получить более мелкие капли и более равномерное распределение. На основе соотношения Райяна и Панди [2001], в котором учитываются физико-химические свойства жидкости, а также ультразвуковые свойства распылителя (амплитуда, частота, площадь вибрирующей поверхности), было проведено четкое моделирование гидродинамики процесса распылительной сушки в прямоточной цилиндро-конической камере. Результаты сопоставлялись с обычным механическим распылением. Модельные прогнозы подтверждены сопоставлением с литературными данными по скоростным и температурным полям для цилиндро-конической камеры. Поскольку ультразвуковое сопло дает низкую начальную скорость и равномерное распыление капель, для моделирования сушки распылением использовались различные скорости капель (0,014; 5,59 и 59,0 м/с) и средние размеры капель (10,0; 30,0; 50,0; 70,0; 90,0; 110,0 мкм). Обсуждаются преимущества и ограничения при использовании ультразвукового распылителя по сравнению с обычными распылителями.

Modellierung der Spritztrocknung bei der Benutzung von Mechanik- und Ultraschallzersträubern – komparative Analyse

Zusammenfassung: Gewöhnliche Mechanikzersträubung gibt die hohe Anfangsgeschwindigkeit den Tropfen und so produziert die große Zerstreuungsgröße. Wird der Strom mit Hilfe der Ultraschallenergie geschafft, kann man die kleineren Tropfen und gleichmäßigere Verteilung erhalten. Auf Grund der Korrelation von Rajan und Pandit [2001], wo die physikalisch-chemischen Eigenschaften der Flüssigkeit und die Ultraschalleigenschaften des Zerstäubers (Amplitude, Frequenz, Vibrationoberfläche) berücksichtigt werden, wurde es die exakte Modellierung der Hydrodynamik des Prozesses der Spritztrocknung in der Zylinder-Kegelkammer durchgeführt. Die Ergebnisse wurden mit der gewöhnlichen Mechanikzerstäubung vergleicht. Modellprognosen sind durch die Vergleichung mit der Litheraturangaben über die Geschwindigkeits- und Temperaturfelder für die Zylinder-Kegelkammer bestätigt. Da die Ultraschalldüse die niedrige Anfangsgeschwindigkeit und die gleichmäßige Tropfenzerstäubung gibt, wurden für die Trocknungsmodellierung verschiedene Tropfengeschwindigkeiten (0,014; 5,59 und 59,0 m/sec) und die durchschnittliche Tropfengröße (10,0; 30,0, 50,0, 70,0, 90,0, 110,0 μm) benutzt. Es werden auch die Vorzüge und die Beschränkungen bei der Benutzung des Ultraschallzerstäubers im Vergleich zu den gewöhnlichen Zerstäubern besprochen.

Simulation du séchage par atomisation avec l'utilisation des atomiseurs mécaniques et ultra-sonores – analyse comparative

Résumé: L'automisation mécanique conventionnelle accorde une haute vitesse initiale aux gouttes ce qui provoque une grande distribition de celles-ci par les dimensions. Si le jet est fait à l'aide de l'énergie ultra-sonore, on peut recevoir les gouttes plus petites et la distribution plus uniforme. A la base de la corrélation Rajan-Pandit [2001] où l'on prend en compte les particularités physiques et chimiques du liquide ainsi que les propriétés ultra-sonores de l'atomiseur (amplitude, fréquence, surface de vibration) on a réalisé la simulation de la computation de la dynamique du

fluide (CDF) pour la prédiction du séchage par atomisation dans la chambre conique et cylindrique à écoulement direct. Les résultats ont été comparés à l'automisation conventionnelle. Les prédictions ont été confirmées par les données littéraires sur les champs de vitesse et de température pour la chambre conique et cylindrique. De différentes vitesses de gouttes ont été utilisées pour la simulation (0,014; 5,59; 59,0 m/sec); ainsi que les dimensions moyennes des gouttes (10,0; 30,0, 50,0, 70,0, 90,0, 110,0 μm). Sont discutés les avantages et les limitations de l'utilisation de l'atomiseur ultra-sonore par comparaison avec les atomiseurs conventionnels.